Hindawi
Journal of Nanomaterials
Volume 2023, Article ID 3995808, 11 pages
https://doi.org/10.1155/2023/3995808

Research Article

On the Role of Bioconvection and Activation Energy for MHD-Stretched Flow of Williamson and Casson Nanofluid Transportation across a Porous Medium Past a Permeable Sheet

M. Eswara Rao,[1] **M. Siva Sankari**,[1] **Ch. Nagalakshmi**,[2] **and S. Rajkumar**[3]

[1]*Department of Mathematics, SIMATS School of Engineering, SIMATS, Chennai 602105, Tamil Nadu, India*
[2]*Department of Mathematics, Bharath Institute of Higher Education and Research, Chennai 600073, Tamil Nadu, India*
[3]*Department of Mechanical Engineering, Faculty of Manufacturing, Institute of Technology, Hawassa University, Hawassa, Ethiopia*

Correspondence should be addressed to S. Rajkumar; ccetraj@gmail.com

Received 3 August 2022; Revised 27 September 2022; Accepted 22 October 2022; Published 2 January 2023

Academic Editor: Omer Alawi

The goal of the current study is to theoretically evaluate the heat and mass transfer behavior of magnetohydrodynamic Casson and Williamson fluids as they pass through a stretched sheet with Brownian and thermophoresis effects. The evolution of high-density heat devices necessitates efficient thermal transportation. For these requirements, the concept of nanofluid plays an active role. This article describes the effects of Cattaneo–Christov. This study introduces new concepts such as motile microorganism bioconvection, non-Fourier heat flux, and activation energy. A Runge–Kutta-based shooting procedure is used to solve the problem. The effects of the relevant parameters on velocity, thermal, concentration, and motile microorganisms are depicted graphically. The computed reduced Nusselt, Sherwood, and motile density numbers are displayed in tables in this study. When compared to the Williamson fluid, the thermal and concentration fields of the Casson fluid are heavily influenced by the parameters.

1. Introduction

Most of the increase in the viscosity of non-Newtonian fluids in modern times is due to trade encroachment. Non-Newtonian fluids transpire not barely in environment, for illustration, mountainside and debris flows, but level in designer mechanization as well as an ample diversity of trade meadows remaining to its vital relevance efficacy in organic material, substances, victuals belongings, and delicate heed yield, among others.

Fluids oscillate in their tackiness, which might differ depending on the speed of twist and assure liquids contain a resilient constituent in temperament, which is alleged as nonfluids [1]. Casson fluid is well-classified when such linear equipment is owed to conventional trim lessening and condensing uniqueness once circumspectly reading the non-Newtonian fluid subclass was studied by Ogunseye et al. [2] and Raju et al. [3]. For its microspore's uniqueness, Casson fluid is non-Newtonian owing to its trim pressure and twist connection. This product is an excellent option for shear-thinning submissions due to its high level of adhesion and yielding resistance to shear. Casson was the originator of the replica, which was ingeniously conceived for ink generation and silicon dispersion.

A mathematical investigation was conducted, and it was concluded that the Casson term drew the drift motion due to increased tackiness. The Casson liquid is one of the most often used viscoelastic non-Newtonian equipment. The energy stint was uncovered to have elevated the Casson rejoinder temperature gradient. Though, the trade worth of Casson liquid can be enlarged once it is collected with Williamson liquid [4], while the Casson and Williamson liquids are intermingled amid manufacturing colloidal nanoparticles in a tacky liquid, the convectional temperature conveys, and the heat conductivity potency of the solvents is augmented for the finest efficiency of nanotechnological and trade products. Bejawada et al. [5] resolute the Williamson and Casson liquids flow past a stretching sheet with heat and mass transfer in the occurrence of heat-reliant heat resource. Magnetohydrodynamics (MHD) is studied by looking at the magnetic properties of electrically conducting liquids.

Explicitly, the magnetic fields acquire an indispensable part in establishing the leads. Owing to this foremost reimbursement, the investigators are incessantly investigating the MHD drifts. MHD drifts are indispensable in a widespread assortment of mechanized and procedural conventions, such as MHD generators, the intend of the nuclear reactor, and flow meters. MHD is a discipline that scrutinizes the drift of electrically accomplishing elucidations in the occurrence of a magnetic field. Abundant inventive and estimated inquiries on usual electrically directing drifts explain that the implication of a magnetic field radically amends their haulage and heat transfer channels. Nuclear influence shrubbery preservation using liquid sodium, the direction force estimate based on liquid probable inequality vertical to motion and the magnetic field, and other tools essential to the study of MHD were analyzed by Rao and Sreenadh [6] and Li et al. [7]. The behavior of the MHD Casson nanoliquid drifted over a permeated sheet was observed by Yahya et al. [8]. The investigators had conferred the brunt of Cattaneo–Christov heat flux on the fluid flow.

Nanofluids are tincture deferments of nanometer dimension elements in a transporter liquid. The nanostructures are deemed in common organization of metals, pewter oxidations, carbon nanospouts and carbides, while the haulers solvent are ethylene and paraffin oil. Lately, nanoliquids change to swift perceive from concocts and researchers since their pervasive procedural, traded, and manufacturing applications like geothermal procedures, power-driven freezing, drug liberation, cancer therapy, heat relocate mechanisms, converter cooling, etc. were discussed by Yousef et al. [9].

Bioconvection refers to the phenomenon in which swimming microorganisms experience an increase in their mobility due to the macroscopic movement of the fluid caused by the spatial fluctuation of density over a region. Gyrotactic microbes in a nanofluid flowing through a porous media causing bioconvection was studied by Ahmad et al. [10]. Williamson Sutterby nanofluid transports due to a stretching surface with a convective boundary, the role of bioconvection and Cattaneo–Christov heat flux was carried out by Yahya et al. [8]. Abdal et al. [11] studied the investigation of the MHD stretched flow of Williamson Maxwell nanofluid through a porous matrix over a penetrated sheet while taking into account bioconvection and activation energy.

The microorganisms that move on their own tend to move the base fluid in a certain direction, creating a bioconvective stream. Different forms of motile microbes, such as those that move via gyrotactic motion, negative gravitaxis, or chemotactic chemicals, have been identified. Awan et al. [12] studied the effects of bioconvection on the flow of Williamson nanofluids caused by an exponentially increasing heat source and a motile microbe over a stretching sheet. Nanobioconvective Williamson fluid that allows for bacteria to swim in the bloodstream was studied by Rana et al. [13]. Williamson nanofluid bioconvection radiative flow across a vertical-stretched cylinder with activation energy and swimming microorganisms in a numerical simulation was explored by Zhang et al. [14].

When compared to motile microbes, the nanoparticles are not self-driven; rather, their motion is influenced by Brownian motion and the thermophoresis effect. Thermophoresis and Brownian motion's effects on thermally and chemically reactive substances flow of Casson nanofluid over a sheet that is being linearly stretched were studied by Tawade et al. [15]. Kumaran and Sandeep [16] studied the parabolic motion of multicomponent, multihybrid (MHD) Casson–Williamson fluids with a Brownian moment and thermophoresis. Thermophoresis and Brownian motion's effects on the heat transfer and entropy formation in nanofluids were discussed by Mahmoodi and Kandelousi [17]. In a suspension of gyrotactic microorganisms over an incline-stretched sheet, the thermo solutal Marangoni effect on bioconvection has been seen by Kairi et al. [18]. If the nanoparticle concentration is low, bioconvection in the nanofluids should be possible because the nanoparticles will not be able to cause a significant increase in the viscosity of the base fluid.

The influence of bioconvection of microorganism for two different drifts of Casson nanofluid and Williamson nanofluid is rarely deliberated in the present article. It aids to deal with the probable subsiding of nanoentities, and thus enrichment of thermal conductivity of the common liquids can be recognized. The novelty of this work affects Cattaneo–Christov heat flux, bioconvection, and activation energy. The buoyancy effects and magnetic field strength impart differentiated stimulus on drift temperature and concentration features. The character of these valuable and workable physical features for two substantial non-Newtonian liquids is counted and their comparative upshots benefit widen our understanding and utilization of these drifts. Utilization of similarity transmutes enables to yield numerical solution of nonlinear coupled system with the execution of Runge–Kutta process and shooting procedure. By exploiting the parametric progress of bioconvection, nanofluid slips, and Cattaneo–Christov factor, the findings are estimated for Casson liquid and Williamson liquid. These outcomes are valuable for thermal management of heat exchangers of the evolving machineries.

2. Outline of the Problem's Mathematical Analysis

A steady two-dimensional surge of Casson and Williamson nanofluids among activation energy and Cattaneo–Christov dissemination entrenched in a porous medium is deliberated in the continuation of biotransformation microfollicles. The liquids drift remaining to a stretching sheet, the wall velocity is $U_w = D_x$, D is stretching persistent. U_w is the stretching velocity of sheet along x-axis. It is reputed that the actions of the drifts rectilinear remain to the impervious stretching sheet. Here, u_a and v_b are the velocities of liquids drift along x-axis and y-axis, respectively. The T, C, and N values in Figure 1 represent the fluid temperature, microbial concentration, and density, respectively, at close proximity to the sheet. We did not stipulate an interior temperature foundation other than the fact that the reaction between substances is first order. We also restrained fractious propagation

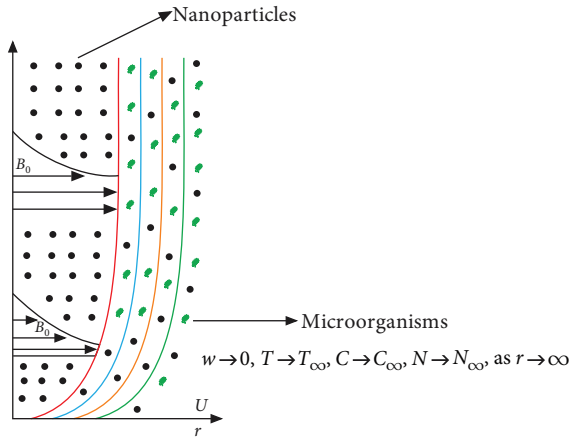

FIGURE 1: Geometry of the problem figure.

possessions by Brownian effort and thermophoresis. We disregarded tacky intemperance and persuaded magnetic field possessions. By the expectations detailed above, the governing equivalence in positions of similarity inconstant can be articulated in the following equations [11].

$$\frac{\partial u_a}{\partial x} + \frac{\partial v_b}{\partial x} = 0. \tag{1}$$

$$\begin{aligned} u_a \frac{\partial u_a}{\partial x} + v_b \partial x \frac{\partial v_b}{\partial x} = {} & \upsilon\left(1 + \frac{1}{\beta}\right)\frac{\partial^2 u_a}{\partial y^2} + \sqrt{2}\Gamma \frac{\partial u_a}{\partial y}\frac{\partial^2 u_a}{\partial y^2} \\ & - \frac{\sigma B_0^2 u_a}{\rho} - \frac{\upsilon}{k'} u_a - \left(\frac{1}{\rho}\right)(1 - C_\infty) \\ & \cdot \rho\beta(T - T_\infty) - (\rho_p - \rho) g (C - C_\infty) \\ & - (N - N_\infty) g \gamma((\rho_m - \rho)). \end{aligned} \tag{2}$$

$$\begin{aligned} u_a \frac{\partial T}{\partial x} + v_b \frac{\partial T}{\partial y} = {} & \alpha \frac{\partial^2 T}{\partial y^2} + \frac{\rho_p C_p}{\rho C}\left[D_B \frac{\partial C}{\partial y}\frac{\partial T}{\partial y} + v_b \frac{D_T}{T_\infty}\left(\frac{\partial T}{\partial y}\right)^2\right] \\ & \tau\left[u_a \frac{\partial u_a}{\partial x}\frac{\partial T}{\partial x} + v_b \frac{\partial v_b}{\partial x}\frac{\partial T}{\partial x} + u_a \frac{\partial v_b}{\partial x}\frac{\partial T}{\partial x} + v_b \frac{\partial u_a}{\partial y}\frac{\partial T}{\partial x} + 2u_a v_b \frac{\partial^2 T}{\partial x \partial y} + {u_a}^2 \frac{\partial}{\partial x}\frac{\partial T}{\partial x} + {v_b}^2 \frac{\partial}{\partial y}\frac{\partial T}{\partial y}\right]. \end{aligned} \tag{3}$$

$$\begin{aligned} u_a \frac{\partial C}{\partial x} + v_b \frac{\partial C}{\partial y} = {} & D_B \frac{\partial}{\partial y}\frac{\partial C}{\partial y} + \frac{D_T}{T_\infty}\frac{\partial}{\partial y}\frac{\partial T}{\partial y} - (Kr)^2 (C_w - C_\infty) \\ & \cdot \left(\frac{T}{T_\infty}\right)^m \exp\left(\frac{-E_a}{k_2 T}\right). \end{aligned} \tag{4}$$

$$u_a \frac{\partial N}{\partial x} + v_b \frac{\partial N}{\partial y} + bW_c \frac{\partial}{\partial y}\left(\frac{n}{\Delta C}\frac{\partial C}{\partial y}\right) = D_m \frac{\partial}{\partial y}\frac{\partial N}{\partial y}. \tag{5}$$

$$\begin{aligned} & u_a = u_w = D_x, v_b = v_w, T - T_w(x) = 0, C - C_w(x) = 0, \\ & \quad N - N_w(x) = 0, \text{at } y = 0 \\ & u_a \longrightarrow 0, T \longrightarrow T_\infty, C \longrightarrow C_\infty, N \longrightarrow N_\infty \text{ at } y \longrightarrow \infty. \end{aligned} \tag{6}$$

Using the similar variables,

$$\begin{aligned} \eta = {} & \sqrt{\frac{D}{\upsilon}} y, u_a = Dx f'(\eta), v_b = -\sqrt{D\upsilon} f(\eta), \theta(\eta) \\ = {} & \frac{T - T_\infty}{T_w - T_\infty}, \phi(\eta) = \frac{C - C_\infty}{C_w - C_\infty}, \psi(\eta) = \frac{N - N_\infty}{N_w - N_\infty}. \end{aligned} \tag{7}$$

Equation (1) is gratified and Equations (2)–(6) become,

$$\begin{aligned} & \left(1 + \frac{1}{\beta}\right) f''' - f'2 + f f'' + \lambda f'' f''' - (M + K_P) f' \\ & \quad + \omega(\theta - Nr\varphi - Rb\psi) = 0. \end{aligned} \tag{8}$$

$$\begin{aligned} & \theta'' + prf\theta' + \frac{\mathrm{Nc}}{\mathrm{Le}}\theta'\phi' + \frac{\mathrm{Nc}}{\mathrm{Le}*\mathrm{Nbt}}\theta' 2 \\ & \quad + b(f^2\theta'' + ff'\theta') = 0. \end{aligned} \tag{9}$$

$$\begin{aligned} & \phi'' + \mathrm{Sc}(f\phi') + \left(\frac{1}{\mathrm{Nbt}}\right)\theta' \\ & \quad - \mathrm{Sc}*A\phi(1 + \delta\theta)^m \exp\left(\frac{-E}{1 + \delta\theta}\right) = 0. \end{aligned} \tag{10}$$

$$\psi'' + \mathrm{Lb}(f\psi') - \mathrm{pe}[\phi''(\psi + \Omega) + \psi'\phi'] = 0. \tag{11}$$

$$\begin{aligned} & f(0) = S, f'(0) = 1, \theta(0) = 1, \phi(0) = 1, \text{at } \eta = 0, \\ & f'(\infty) \longrightarrow 0, \theta(\infty) \longrightarrow 0, \phi(\infty) \longrightarrow 0, \psi \longrightarrow \infty, \text{as } \eta \longrightarrow \infty. \end{aligned} \tag{12}$$

The nondimensional constraints are in their particular order,

where,

$$\beta = \lambda_1 D, M = \frac{\sigma B^2{}_o}{D\rho}, K_P = \frac{\upsilon}{k_1 D}, \omega = \frac{\beta_1 g(1 - C_\infty)(T_w - T_\infty)}{D^2 x}. \tag{13}$$

$$\mathrm{Nr} = \frac{(\rho_p - \rho)(C_w - C_\infty)}{\beta_1 \rho (1 - C_\infty)(T_w - T_\infty)}, \mathrm{Rb} = \frac{(\rho_m - \rho)\gamma N_\infty}{(1 - C_\infty)\rho\beta T_\infty}. \tag{14}$$

$$b = \tau_1 D, \mathrm{Sc} = \frac{\upsilon}{D_B}, A = \frac{k^2 r}{D}, \delta = \frac{T_w - T_\infty}{T_\infty}, E = \frac{E_a}{k_2 T_\infty}. \tag{15}$$

$$\mathrm{Lb}=\frac{\upsilon}{D_m},\ \mathrm{Pe}=\frac{b_1 Wc}{D_m},\ \Omega=\frac{N_\infty}{N_\mathrm{w}-N_\infty},\ S=\frac{-\upsilon_\mathrm{w}}{\sqrt{D\upsilon}}. \tag{16}$$

$$\mathrm{Pr}=\frac{\upsilon}{\alpha},\ \mathrm{Le}=\frac{\alpha}{D_\mathrm{B}},\ \mathrm{Nbt}=\frac{D_\mathrm{B}T_\infty(C_\mathrm{w}-C_\infty)}{D_\mathrm{T}(T_\mathrm{w}-T_\infty)}. \tag{17}$$

The objective quantities are declared as: Cf_x, viscous drag coefficient; Nu_x, local Nusselt number; Sh_x, local Sherwood number; and Nn_x, local density of microfollicles are known in Equation (18).

$$\mathrm{Cf}_x=\frac{\tau_\omega}{\rho U^2 w},\ \mathrm{Nu}_x=\frac{xq_w}{k(T_\mathrm{w}-T_\infty)},\ \mathrm{Sh}_x=\frac{xq_m}{D_\mathrm{B}(C_\mathrm{w}-C_\infty)},\ \mathrm{Nn}_x=\frac{xq_n}{D_m(N_\mathrm{w}-N_\infty)}, \tag{18}$$

where τ_w, q_w, q_m, and q_n denote shear stress, surface heat flux, surface mass flux, and motile microfollicles flux are given by (at $y=0$),

$$\tau_w=\mu(1+\beta)\left(1+\frac{\Gamma}{2}\frac{\partial u_a}{\partial y}\right)\frac{\partial u_a}{\partial y},\ q_w=-k\frac{\partial T}{\partial y},\ q_m=-D_\mathrm{B}\frac{\partial C}{\partial y},\ q_n=-D_m\frac{\partial N}{\partial y}. \tag{19}$$

On solving these quantities with the help of known similarity transformation, we acquire,

$$\mathrm{Cf}_x(\mathrm{Re}_x)^{-1/2}=(1+\beta)\left(f''(0)+\frac{\lambda}{2}f''(0)^2,\mathrm{Nu}_x(\mathrm{Re}_x)^{-1/2}=-\theta'(0)\right),\ \mathrm{Sh}_x(\mathrm{Re}_x)^{-1/2}=-\phi'(0),\mathrm{Nn}_x(\mathrm{Re}_x)^{-1/2}=-\psi'(0) \tag{20}$$

where $(\mathrm{Re}_x)=xU_w/\nu$ is the local Reynolds number.

3. Solution Procedure

For numerical results, the Runge–Kutta method of order four and the shooting technique are used to solve the nonlinear ordinary differential Equations (8)–(11) with the given boundary conditions (12). To use this method, the new variable is written as follows [11]:

$$\begin{aligned}
h_1' &= h_2\\
h_2' &= h_3\\
h_3' &= (1/(1+(1/\beta))(h_2^2)+\lambda h_3 h_3'+(M+K_\mathrm{P})h_2-w(\theta-\mathrm{Nr}\phi-\mathrm{Rb}\chi)\\
h_4' &= h_5\\
h_5' &= -prh_1h_5-\left(\frac{\mathrm{Nc}}{\mathrm{Le}}\right)h_5h_7-\left(\frac{\mathrm{Nc}}{\mathrm{Le}*\mathrm{Nbt}}\right)h_5^2-b(h_1^2h_5'+h_1h_1'h_4')\\
h_6' &= h_7\\
h_7' &= -\mathrm{Sc}(h_1h_6')-\left(\frac{1}{\mathrm{Nbt}}\right)h_7'-\mathrm{Sc}*\mathrm{Ah}_6(1+\delta h_4)^m\exp\left(\frac{-E}{1+\delta h_4}\right)\\
h_8' &= h_9\\
h_9' &= \mathrm{Pe}(h_7'(\chi+\Omega)+h_8'h_6')-\mathrm{Lb}(h_1h_8').
\end{aligned} \tag{21}$$

4. Results and Discussion

This exertion obtainable is a representation of non-Newtonian Casson–Williamson nanoliquid surge wizened by the momentum, energy, and concentration equation and persuaded by the magnetic field, biotransformation, porous medium, microfollicle, heat creation, and chemical reaction. We exploit the fourth-order Runge–Kutta amalgamation design and a shooting approach to unravel the structure of extremely erratic ordinary differential Equations (11), (12), and (18) in concert with the boundary conditions (19) and (20), which articulate that problem. The tabular methods are used to show the numerical investigations. The influence of nanoliquid physical strictures on heat and mass transference tariffs, as well as the local drag friction factor, local Nusselt number, local Sherwood number, and local motile density number are also calculated and obtainable in Tables 1 and 2. The upshots of liquid strictures on the Casson and Williamson nanoliquid velocity $f'(\eta)$, temperature $\theta(\eta)$, concentration $\varphi(\eta)$, and motile density contour $\chi(\eta)$ are obtainable explicitly and deliberated in this sector.

5. Velocity Profile

For different data of magnetic parameter, M, the effect of velocity profile has been exposed in Figure 2(a). It is observed that as M goes up, $f'(\eta)$ goes down. This is because a strong magnetic field helps produce a force called the Lorentz force, which slows down the drift of liquid. It is clear that Lorentz force had more of an upshot on Williamson fluid than on Casson liquid.

The enhanced porosity parameter K_P, as shown in Figure 2(b), retards the flow velocity because K_P has the ability to produce fluid flow resistance.

Figure 2(c) presents the result of the mixed transformation stricture applied to $f'(\eta)$ for Williamson and Casson nanofluids. The higher values of the mixed convection stricture cause an upsurge as a result of the stronger buoyancy force.

Figures 2(d) and 2(e) explain the characteristics of the bioconvection Rayleigh number (Rb) and the buoyancy ratio parameter (Nr) as they are related to $f'(\eta)$.

Changing both parameters causes $f'(\eta)$ to decline. Physically, both values are related to buoyancy ratio forces that resist the motion of the two fluids.

6. Temperature

Figure 3(a) illustrates the temperature field for a range of values of M. When the values of M go up, the temperature spreads out more. Physically, an increase in M generated the flow-resisting force (Lorentz force). This force has a propensity to reveal $\theta(\eta)$. Additionally, it is shown that the thermal boundary layer of Casson fluid is significantly influenced by the Lorentz force compared to that of Williamson fluid.

Figure 3(b) presents an illustration of the effects that b has on $\theta(\eta)$. By increasing the Cattaneo–Christov parameter b, $\theta(\eta)$ is decreased. Consequently, Casson fluid diffuses

Table 1: Values of $\mathrm{Cf}\sqrt{\mathrm{Re}_x}$, $\mathrm{Nu}_x/\sqrt{\mathrm{Re}_x}$, $\mathrm{Sh}_x/\sqrt{\mathrm{Re}_x}$, and $\mathrm{Nn}_x/\sqrt{\mathrm{Re}_x}$ for values of M, K_P, w, Nr, Rb, Pr, Nc, Nbt, b, E, A, Le, Ω, Lb, and Pe (for Williamson fluid ($\lambda = 0.2$ and $\beta = \infty$)).

M	K_P	w	Nr	Rb	b	Le	Pr	Nc	E	A	D	Lb	Pe	$\mathrm{Cf}\sqrt{\mathrm{Re}_x}$	$\mathrm{Nu}_x/\sqrt{\mathrm{Re}_x}$	$\mathrm{Sh}_x/\sqrt{\mathrm{Re}_x}$	$\mathrm{Nn}_x/\sqrt{\mathrm{Re}_x}$
0.0														1.263533	0.122290	0.794755	0.219625
0.3														1.384584	0.122745	0.781862	0.219258
	0.0													1.177620	0.121745	0.804716	0.219923
	0.5													1.384584	0.122745	0.781862	0.219258
		0.1												1.384584	0.122745	0.781862	0.219258
		0.3												1.384584	0.122745	0.781862	0.219258
			1											1.384584	0.122745	0.781862	0.219258
			2											1.433462	0.122935	0.75578	0.219072
				.1										1.384584	0.122745	0.781862	0.219258
				2										1.456039	0.123362	0.769658	1.456039
					1									1.384584	0.122745	0.781862	0.219258
					2									1.383860	0.113154	0.792164	0.792164
						0.1								1.384584	0.122745	0.781862	0.219258
						0.2								1.391330	0.195785	0.703157	0.226310
							0.5							1.384584	0.122745	0.781862	0.219258
							1.0							1.393963	0.186041	0.703528	0.225622
								0.1						1.384584	0.122745	0.781862	0.219258
								0.5						1.358337	0.001637	0.974657	0.205305
									1					1.384584	0.122745	0.781862	0.219258
									2					1.385067	0.123438	0.759229	0.221479
										0.1				1.384584	0.122745	0.781862	0.219258
										0.5				1.381695	0.118669	0.929260	0.204704
											0.0			1.384475	0.122745	0.781892	0.221915
											0.05			1.384584	0.122745	0.781862	0.219258
												0.1		1.384584	0.122745	0.781862	0.219258
												0.2		1.382600	0.122682	0.782490	0.252241
													0.0	1.382244	0.122567	0.787378	0.281991
													0.1	1.384495	0.122617	0.786778	0.218770

more heat than Williamson fluid, and the temperature curve for Casson fluid is steeper than that for Williamson fluid. λ is obviously a ratio between buoyant forces and viscous forces. Consequently, a small change induces a decrease in the $\theta(\eta)$.

Figure 3(c) demonstrates the effect of the Lewis number Le on $\theta(\eta)$. $\theta(\eta)$ depreciates as a result of its direct association with the diffusivity of mass, which leads to a decrease in the temperature distribution.

The influence of Pr is shown as $\theta(\eta)$ in Figure 3(d). It is obvious that raising Pr values results in a decrease in $\theta(\eta)$. Physically, it results from Pr's opposite relationship to thermal diffusivity.

The relationship between Nc and $\theta(\eta)$ is illustrated in Figure 3(e); a rise in Nc results in an increase in $\theta(\eta)$.

7. Concentration

The concentration fields are shown in Figure 4(a) for various magnetic field parameter values. The concentration distribution $\varphi(\eta)$ is enhanced by raising the values of the magnetic field parameter. Physically, increasing the magnetic field parameter caused the flow to experience a resistive force (Lorentz force). This force has a propensity to make the concentration field visible. Additionally, it is shown that, in contrast to Williamson fluid, the concentration boundary layers of Casson fluid are strongly influenced by the Lorentz force.

As shown in Figure 4(b), an upsurge in the activation energy E persuades an upsurge in $\varphi(\eta)$.

Figure 4(c) depicts a decline in $\varphi(\eta)$ as the chemical reaction rate parameter A is exceeded. Larger inputs of A result in a more rapid chemical reaction that decreases $\varphi(\eta)$ while the increase in A generates greater resistance to the flow of Casson fluids compared to Williamson fluids.

With the exceeding of the Lewis number Le, $\varphi(\eta)$ decreases as shown in Figure 4(d). In addition, a decrease in mass diffusivity makes Casson fluid less resistant to flow than Williamson fluid.

7.1. Motile Density. With an increase in M, the motile density profile $\chi(\eta)$ becomes more pronounced in Figure 5(a). It is a result of the flow slowing. The motile density profile $\chi(\eta)$ is increased as a result of the curves produced by M.

By raising the value of the microorganism difference parameter, which is shown in Figure 5(b), it also exhibits an addition.

Table 2: Values of $\mathrm{Cf}\sqrt{\mathrm{Re}_x}$, $\mathrm{Nu}_x/\sqrt{\mathrm{Re}_x}$, $\mathrm{Sh}_x/\sqrt{\mathrm{Re}_x}$, and $\mathrm{Nn}_x/\sqrt{\mathrm{Re}_x}$ for values of M, K_P, w, Nr, Rb, Pr, Nc, Nbt, b, E, A, Le, Ω, Lb, and Pe (for Casson fluid ($\beta = 2.0$ and $\lambda = 0$)).

M	K_P	W	Nr	Rb	b	Le	Pr	Nc	E	A	D	Lb	Pe	$\mathrm{Cf}\sqrt{\mathrm{Re}_x}$	$\mathrm{Nu}_x/\sqrt{\mathrm{Re}_x}$	$\mathrm{Sh}_x/\sqrt{\mathrm{Re}_x}$	$\mathrm{Nn}_x/\sqrt{\mathrm{Re}_x}$
0.0														1.067904	0.121172	0.815205	0.220206
0.3														1.161474	0.122041	0.802901	0.219814
	0.0													1.000718	0.120361	0.824575	0.220521
	0.5													1.161474	0.122041	0.802901	0.219814
		0.1												1.161474	0.122041	0.802901	0.219814
		0.3												1.161474	0.122041	0.802901	0.219814
			1											1.161474	0.122041	0.802901	0.219814
			2											1.195597	0.122355	0.798100	0.219658
				.1										1.161474	0.122041	0.802901	0.219814
				2										1.212987	0.122944	0.792657	0.219425
					1									1.161474	0.122041	0.802901	0.219814
					2									1.160626	0.110194	0.816000	0.218647
						0.1								1.161474	0.122041	0.802901	0.219814
						0.2								1.166217	0.192633	0.728983	0.226516
							0.5							1.161474	0.122041	0.802901	0.219814
							1.0							1.168636	0.185751	0.726016	0.226118
								0.1						1.161474	0.122041	0.802901	0.219814
								0.5						1.142100	0.001887	0.986820	0.206183
									1					1.161474	0.122041	0.802901	0.219814
									2					1.161812	0.122699	0.781078	0.221961
										0.1				1.161474	0.122041	0.802901	0.219814
										0.5				1.159439	0.118134	0.945955	0.205660
											0.0			1.161389	0.122038	0.802928	0.222573
											0.05			1.161474	0.122041	0.802901	0.219814
												0.1		1.161474	0.122041	0.802901	0.219814
												0.2		1.159819	0.121962	0.803490	0.255569
													0.0	1.159738	0.121980	0.803427	0.284535
													0.1	1.161474	0.122041	0.802901	0.219814

Figure 5(c) illustrates the outcomes of Peclet number Pe. A greater Peclet number decreases microorganism diffusivity. The increase in Peclet number Pe reduces the microorganism boundary layer thickness and motile density profile $\chi(\eta)$.

Figure 5(d) depicts the results of the Lewis number Lb. Furthermore, it is evident that a lower value of $\chi(\eta)$ for the spread of microorganisms results from a bigger value of Lb.

8. Conclusions

This paper investigates the significance of magnetic field, biotransformation, and activation energy for Williamson and Casson nanofluid on a porous prolonged pane with Cattaneo–Christov dissemination. The key findings of this study are as follows:

(1) It is scrutinized that for the superior efforts of magnetic stricture M and porous its stricture, the velocity diminishes

(2) Among the intensifying significances of Rayleigh number Rb, buoyancy ratio stricture Nr, velocity moderates, while conflicting conduct be revealed for w

(3) Temperature diminishes amid the heckling significances of Cattaneo–Christov strictures b, Lewis number Le, and Prandtl number Pr

(4) Casson fluid is further exaggerated with these austere than Williamson fluid. On contrary, M and Nc show opposite behavior for it

(5) Le sources reduction into concentration, while these strictures seize hefty values. On further dispense, the concentration demonstrates conflicting conduct for E

(6) For motile density contour disparate strictures, i.e., $\Omega(D)$ and Peclet number. Pe articulates extra upshot for Casson fluids as evaluated to Williamson fluids

(7) Skin friction coefficient enhanced for β, M, K_P, Nr, and Rb while decreased down for λ and ω

(8) Nusselt number reduces when uplifting the parameter Nc, while it increases for Pr, Nbt, and b

(9) Sherwood number increases for Sc, A, δ, and n while it reduces when uplifting the parameter E

(10) Motile density number increases for Lb, $\Omega(D)$, and Pe

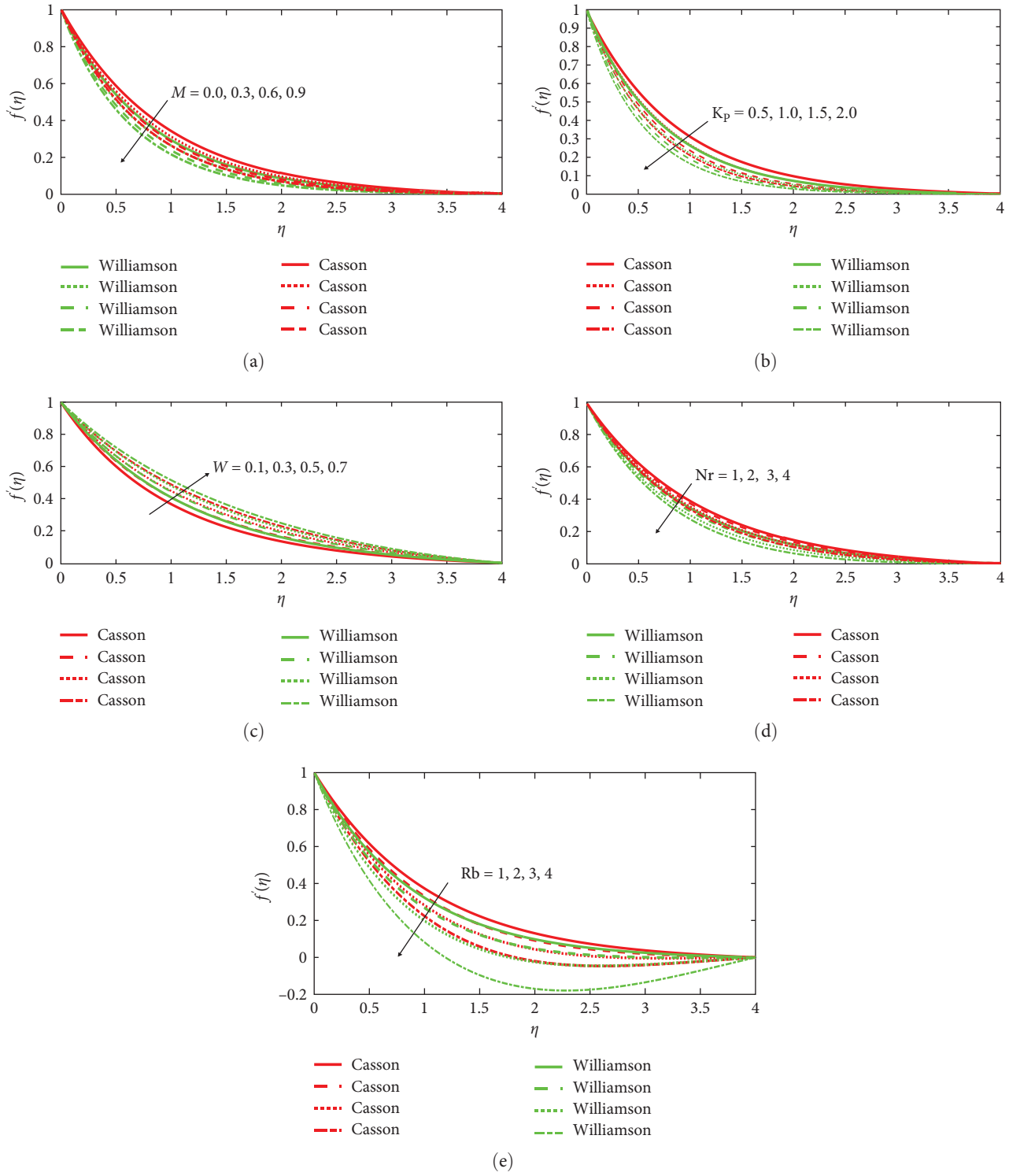

FIGURE 2: (a) Influence of M on $f'(\eta)$. (b) Influence of K_P on $f'(\eta)$. (c) Influence of w on $f'(\eta)$. (d) Influence of Nr on $f'(\eta)$. (e) Influence of Rb on $f'(\eta)$.

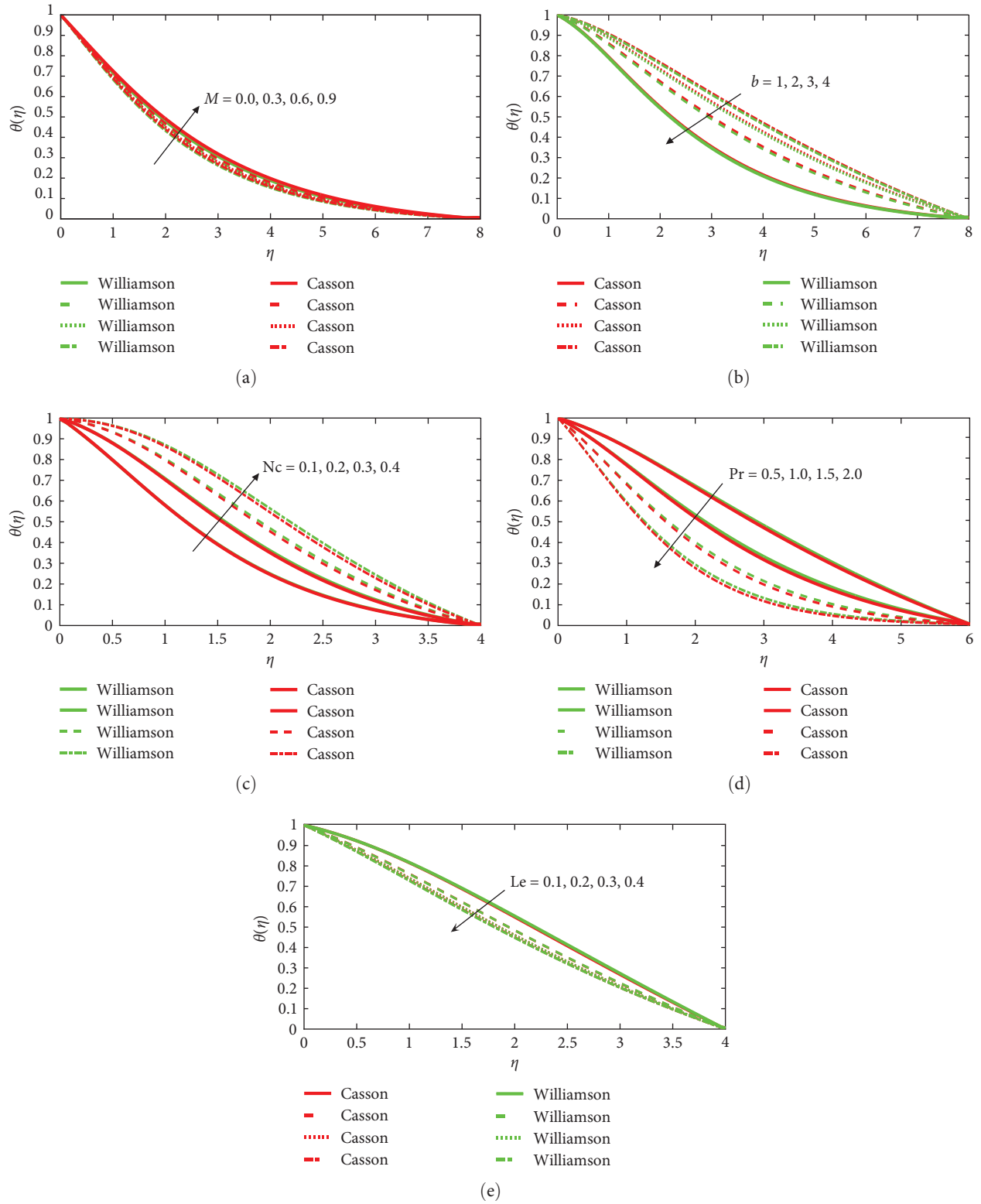

FIGURE 3: (a) Influence of M on $\theta(\eta)$. (b) Influence of b on $\theta(\eta)$. (c) Influence of Le on $\theta(\eta)$. (d) Influence of Pr on $\theta(\eta)$. (e) Influence of Le on $\theta(\eta)$.

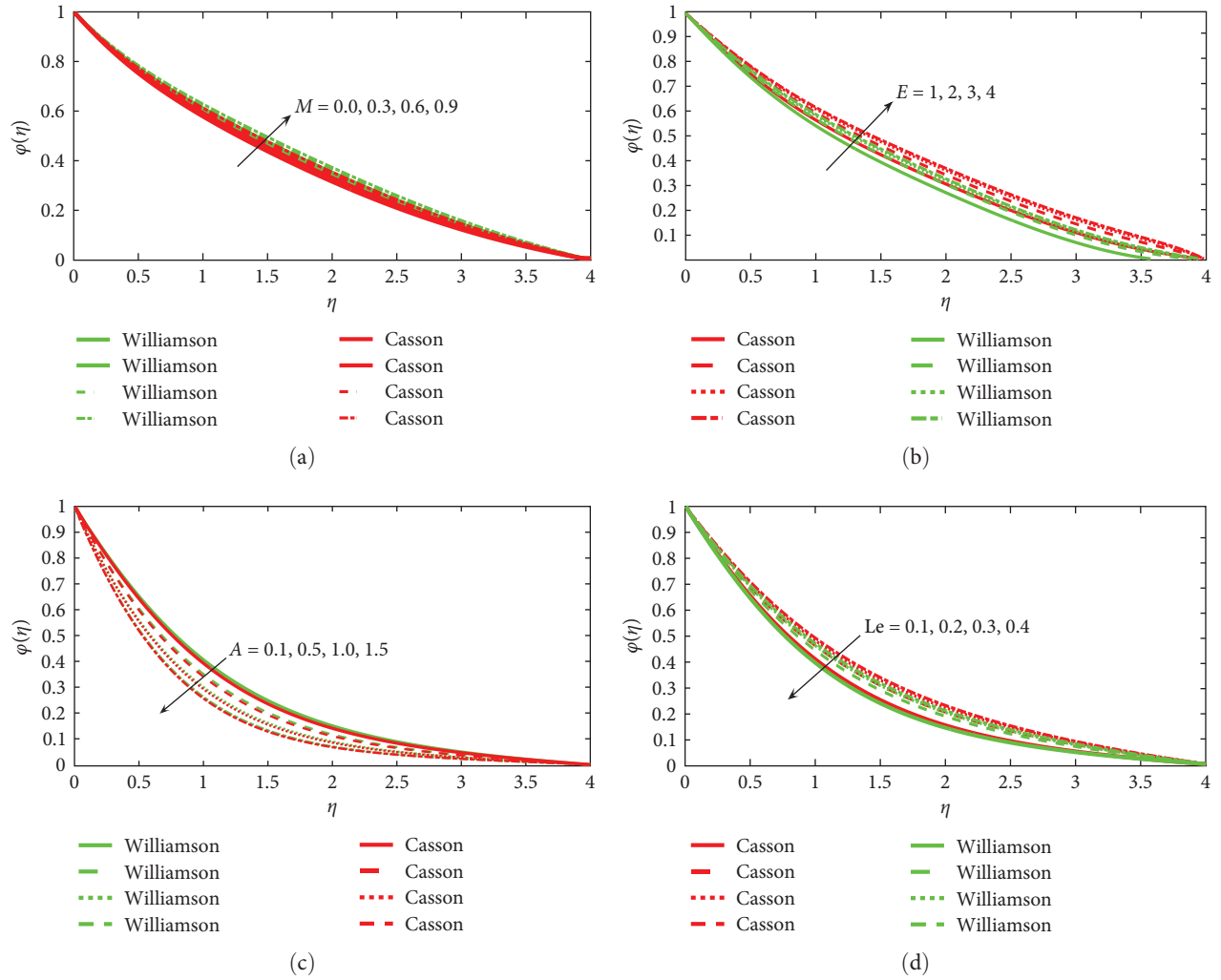

Figure 4: (a) Influence of A on $\varphi(\eta)$. (b) Influence of E on $\varphi(\eta)$. (c) Influence of A on $\varphi(\eta)$. (d) Influence of Le on $\varphi(\eta)$.

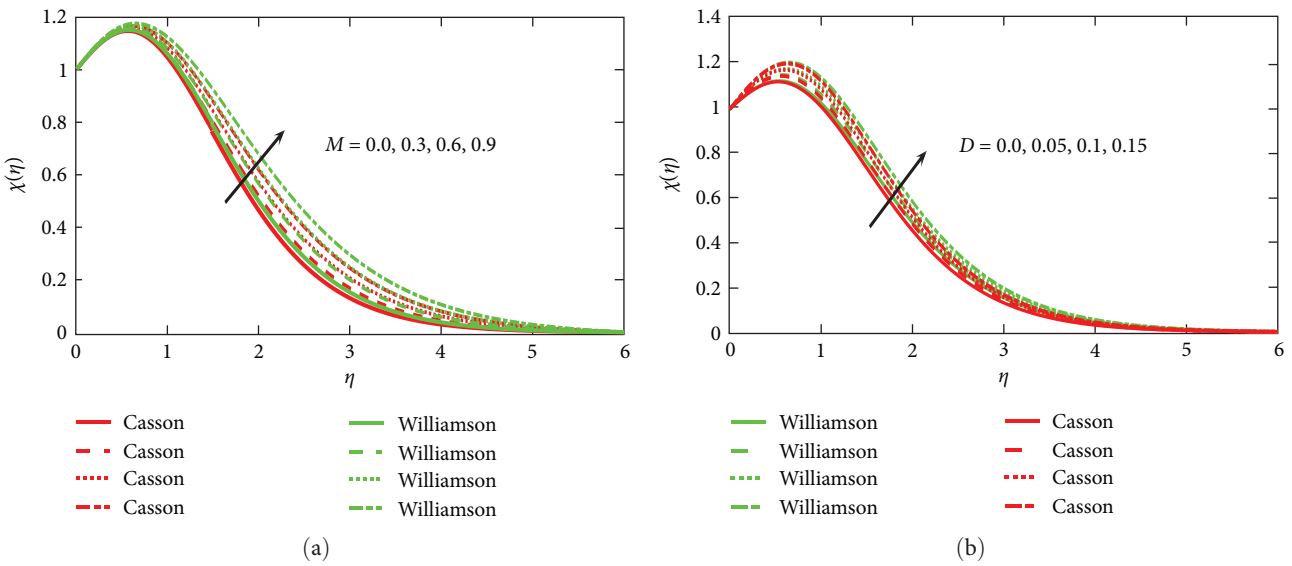

Figure 5: Continued.

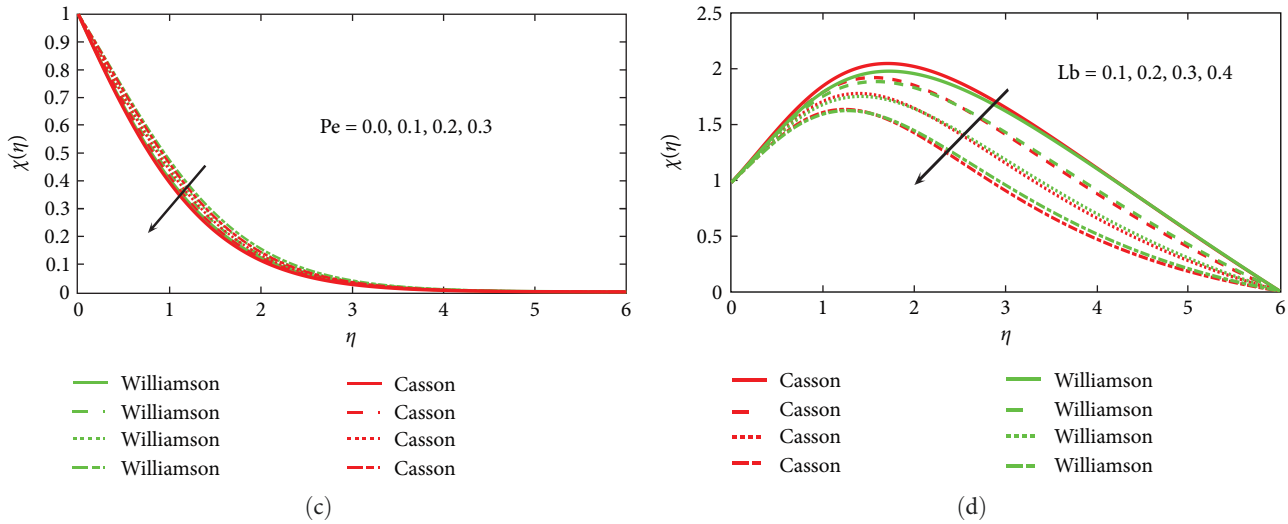

FIGURE 5: (a) Influence of M on $\chi(\eta)$. (b) Influence of D on $\chi(\eta)$. (c) Influence on Pe on $\chi(\eta)$. (d) Influence of Lb on $\chi(\eta)$.

Nomenclature

n: Power law index
M: Magnetic parameter
b: Cattaneo–Christov parameter
B_0: Magnetic field strength
K_P: Porosity parameter
Pr: Prandtl number
Sc: Schmidt number
Nb: Brownian parameter
Nc: Thermophoresis parameter
D_B: Brownian diffusion constant
D_T: Thermophoresis diffusion coefficient
Cf_x: Skin friction coefficient
Sh_x: Sherwood number
Nu_x: Nusselt number
Nn_x: Density of microorganism
α: Thermal diffusivity of base fluid
μ: Viscosity of fluid
ψ: Stream function
ν: Kinematic viscosity
σ: Electrical conductivity
ρ: Density of fluid
ρ_p: Nanoparticles density
γ: Spin gradient velocity
Γ: Material time constant
δ: Unsteadiness parameter
C: Concentration of nanoparticles
T: Temperature of nanoparticles
C_P: Specific heat at constant pressure
C_w: Nanoparticles concentration at wall
T_w: Wall constant temperature.

Data Availability

All data are included in this research article.

Conflicts of Interest

The authors declare that they have no conflicts of interest.

Acknowledgments

The authors acknolwedge S. Rajkumar, Department of Mechanical Engineering, Faculty of Manufacturing, Institute of Technology, Hawassa University, Ethiopia to carry out this work.

References

[1] N. I. Nima, S. O. Salawu, M. Ferdows, M. D. Shamshuddin, A. Alsenafi, and A. Nakayama, "Melting effect on non-Newtonian fluid flow in gyrotactic microorganism saturated non-Darcy porous media with variable fluid properties," *Applied Nanoscience*, vol. 10, pp. 3911–3924, 2020.

[2] H. A. Ogunseye, S. O. Salawub, and E. O. Fatunmbic, "A numerical study of MHD heat and mass transfer of a reactive Casson–Williamson nanofluid past a vertical moving cylinder," *Partial Differential Equations in Applied Mathematics*, vol. 4, Article ID 100148, 2021.

[3] C. S. K. Raju, N. Sandeep, Md. E. Ali, and A. O. Nuhait, "Heat and mass transfer in 3-D MHD Williamson–Casson fluids flow over a stretching surface with non-uniform heat source/sink," *Thermal Science*, vol. 23, no. 1, pp. 281–293, 2019.

[4] A. Zeeshan, O. U. Mehmood, F. Mabood, and F. Alzahrani, "Numerical analysis of hydromagnetic transport of Casson nanofluid over permeable linearly stretched cylinder with Arrhenius activation energy," *International Communications in Heat and Mass Transfer*, vol. 130, Article ID 105736, 2022.

[5] S. G. Bejawada, Y. D. Reddy, W. Jamshed, K. S. Nisar, A. N. Alharbi, and R. Chouikh, "Radiation effect on MHD Casson fluid flow over an inclined non-linear surface with chemical reaction in a Forchheimer porous medium," *Alexandria Engineering Journal*, vol. 61, no. 10, pp. 8207–8220, 2022.

[6] M. E. Rao and S. Sreenadh, "MHD boundary layer flow of Casson fluid over a stretching/shrinking sheet through porous medium," *Chemical and Process Engineering Research*, vol. 47, pp. 21–33, 2017.
[7] Y.-X. Li, M. H. Alshbool, Y.-P. Lv, I. Khan, M. Riaz Khan, and A. Issakhov, "Heat and mass transfer in MHD Williamson nanofluid flow over an exponentially porous stretching surface," *Case Studies in Thermal Engineering*, vol. 26, Article ID 100975, 2021.
[8] A. U. Yahya, N. Salamat, D. Habib, B. Ali, S. Hussain, and S. Abdal, "Implication of bio-convection and Cattaneo–Christov heat flux on Williamson Sutterby nanofluid transportation caused by a stretching surface with convective boundary," *Chinese Journal of Physics*, vol. 73, pp. 706–718, 2021.
[9] N. S. Yousef, A. M. Megahed, N. I. Ghoneim, M. Elsafi, and E. Fares, "Chemical reaction impact on MHD dissipative Casson–Williamson nanofluid flow over a slippery stretching sheet through porous medium," *Alexandria Engineering Journal*, vol. 61, no. 12, pp. 10161–10170, 2022.
[10] S. Ahmad, M. Ashraf, and K. Ali, "Bioconvection due to gyrotactic microbes in a nanofluid flow through a porous medium," *Heliyon*, vol. 6, no. 12, Article ID e05832, 2020.
[11] S. Abdal, I. Siddique, D. Alrowaili, Q. Al-Mdalla, and S. Hussain, "Exploring the magnetohydrodynamic stretched flow of Williamson Maxwell nanofluid through porous matrix over a permeated sheet with bioconvection and activation energy," *Scientifc Reports*, vol. 12, Article ID 278, 2022.
[12] A. U. Awan, S. A. A. Shah, and B. Ali, "Bioconvection effects on Williamson nanofluid flow with exponential heat source and motile microorganism over a stretching sheet," *Chinese Journal of Physics*, vol. 77, pp. 2795–2810, 2022.
[13] B. M. J. Rana, S. M. Arifuzzaman, S. Islam et al., "Swimming of microbes in blood flow of nano-bioconvective Williamson fluid," *Thermal Science and Engineering Progress*, vol. 25, Article ID 101018, 2021.
[14] X. Zhang, D. Yang, M. I. Ur Rehman, A. A. Mousa, and A. Hamid, "Numerical simulation of bioconvection radiative flow of Williamson nanofluid past a vertical stretching cylinder with activation energy and swimming microorganisms," *Case Studies in Thermal Engineering*, vol. 33, Article ID 101977, 2022.
[15] J. V. Tawade, C. N. Guled, S. Noeiaghdam, U. Fernandez-Gamiz, V. Govindan, and S. Balamuralitharan, "Effects of thermophoresis and Brownian motion for thermal and chemically reacting Casson nanofluid flow over a linearly stretching sheet," *Results in Engineering*, vol. 15, Article ID 100448, 2022.
[16] G. Kumaran and N. Sandeep, "Thermophoresis and Brownian moment effects on parabolic flow of MHD Casson and Williamson fluids with cross diffusion," *Journal of Molecular Liquids*, vol. 233, pp. 262–269, 2017.
[17] M. Mahmoodi and S. Kandelousi, "Effects of thermophoresis and Brownian motion on nanofluid heat transfer and entropy generation," *Journal of Molecular Liquids*, vol. 211, pp. 15–24, 2015.
[18] R. R. Kairi, S. Shaw, S. Roy, and S. Raut, "Thermosolutal Marangoni impact on bioconvection in suspension of gyrotactic microorganisms over an inclined stretching sheet," *Journal of Heat Transfer*, vol. 143, no. 3, Article ID 031201, 2021.